HE 1143

PERGAMON

International Journal of Hydrogen Energy 000 (2000) 000–000

International Journal of HYDROGEN ENERGY

www.elsevier.com/locate/ijhydene

Observation of extreme ultraviolet hydrogen emission from incandescently heated hydrogen gas with strontium that produced an anomalous optically measured power balance

Randell L. Mills *, Mark Nansteel, Ying Lu

BlackLight Power, Inc., 493 Old Trenton Road, Cranbury, NJ 08512, USA

Abstract

We report the observation of intense extreme ultraviolet (EUV) emission from incandescently heated atomic hydrogen and atomized strontium. It has been reported that intense EUV emission was observed at low temperatures (e.g. $\approx 10^3$ K) from atomic hydrogen and certain atomized elements or certain gaseous ions which ionize at integer multiples of the potential energy of atomic hydrogen, 27.2 eV [1–5]. Strontium ionizes at integer multiples of the potential energy of atomic hydrogen. Typically the emission of extreme ultraviolet light from hydrogen gas is achieved via a discharge at high voltage, a high-power inductively coupled plasma, or a plasma created and heated to extreme temperatures by RF coupling (e.g. $> 10^6$ K) with confinement provided by a toroidal magnetic field. The observed plasma formed at low temperatures (e.g. $\approx 10^3$ K) from atomic hydrogen generated at a tungsten filament that heated a titanium dissociator and atomic strontium which was vaporized from the metal by heating. No emission was observed when sodium, magnesium, or barium replaced strontium or with hydrogen or strontium alone. The power balance of a gas cell having atomized hydrogen and strontium was measured by integrating the total light output corrected for spectrometer system response and energy over the visible range. A control cell was identical except that sodium replaced strontium. In this case, 4000 times the power of the strontium cell was required in order to achieve that same optically measured light output power. A plasma formed at a cell voltage of about 250 V in the cell with hydrogen alone and in the cell with hydrogen and sodium; whereas, a plasma formed in the strontium cell at the extremely low voltage of about 2 V.

1. Introduction

A historical motivation to analyze EUV emission from a hydrogen gas was that the spectrum of hydrogen was first recorded from the only known source, the Sun [6]. Developed sources that provide a suitable intensity are high-voltage discharge, synchrotron, and inductively coupled plasma generators [7]. An important variant of the later type of source is a tokomak [8]. Fujimoto et al. [9] have determined the cross section for the production of excited hydrogen atoms from the emission cross sections for Lyman and Balmer lines when molecular hydrogen is dissociated into excited atoms by electron collisions. These data were used to develop a collisional-radiative model to be used in determining the ratio of molecular-to-atomic hydrogen densities in tokomak plasmas. Their results indicate an excitation threshold of 17 eV for Lyman α emission. Addition of other gases would be expected to decrease the intensity of hydrogen lines which could be absorbed by the gas. Hollander and Wertheimer [10] found that within a selected range of parameters of a plasma created in a microwave resonator cavity, a hydrogen–oxygen plasma displays an

* Corresponding author. Tel.: +1-609-490-1040; fax: +1-609-490-1066.

E-mail address: rmills@blacklightpower.com (R.L. Mills).

0360-3199/00/$20.00
PII: S0360-3199(00)00098-7

emission that resembles the absorption of molecular oxygen. Whereas, a helium–hydrogen plasma emits a very intense hydrogen Lyman α radiation at 121.5 nm which is up to 40 times more intense than other lines in the spectrum. The Lyman α emission intensity showed a significant deviation from that predicted by the model of Fujimoto et al. [9] and from the emission of hydrogen alone.

We report that a hydrogen plasma is formed at low temperatures (e.g. $\approx 10^3$ K) by reaction of atomic hydrogen with strontium atoms, but not with magnesium, barium, or sodium atoms. In the case of EUV measurements, atomic hydrogen was generated by dissociation at a tungsten filament and at a transition metal dissociator that was incandescently heated by the filament. Strontium atoms were vaporized by heating to form a low vapor pressure (e.g. 1 torr). The kinetic energy of the thermal electrons at the experimental temperature of $\approx 10^3$ K were about 0.1 eV, and the average collisional energies of electrons accelerated by the field of the filament were less than 1 eV. (No blackbody emission was recorded for wavelengths shorter than 400 nm.) Strontium atoms ionize at integer multiples of the potential energy of atomic hydrogen and caused hydrogen EUV emission; whereas, the chemically similar atoms, magnesium and barium as well as sodium, caused no emission. Helium ions present in the experiment of Hollander and Wertheimer [10] ionize at a multiple of two times the potential energy of atomic hydrogen. The mechanism of EUV emission cannot be explained by the conventional chemistry of hydrogen, but it is predicted by a solution of the Schrodinger equation with a nonradiative boundary constraint put forward by Mills [11].

Mills predicts that certain atoms or ions serve as catalysts to release energy from hydrogen to produce an increased binding energy hydrogen atom called a *hydrino atom* having a binding energy of

$$\text{Binding energy} = \frac{13.6 \text{ eV}}{n^2}, \quad (1)$$

where

$$n = \frac{1}{2}, \frac{1}{3}, \frac{1}{4}, \ldots, \frac{1}{p} \quad (2)$$

and p is an integer greater than 1, designated as $H[a_H/p]$ where a_H is the radius of the hydrogen atom. Hydrinos are predicted to form by reacting an ordinary hydrogen atom with a catalyst having a net enthalpy of reaction of about

$$m \cdot 27.2 \text{ eV}, \quad (3)$$

where m is an integer. This catalysis releases energy from the hydrogen atom with a commensurate decrease in size of the hydrogen atom, $r_n = na_H$. For example, the catalysis of H $\left(n = 1, r_H = a_H\right)$ to $H\left(n = \frac{1}{2}\right)$ releases 40.8 eV, and the hydrogen radius decreases from a_H to $\frac{1}{2}a_H$.

The excited energy states of atomic hydrogen are also given by Eq. (1) except that

$$n = 1, 2, 3, \ldots . \quad (4)$$

The $n = 1$ state is the "ground" state for "pure" photon transitions (the $n = 1$ state can absorb a photon and go to an excited electronic state, but it cannot release a photon and go to a lower-energy electronic state). However, an electron transition from the ground state to a lower-energy state is possible by a nonradiative energy transfer such as multipole coupling or a resonant collision mechanism. These lower-energy states have fractional quantum numbers, $n = 1/\text{integer}$. Processes that occur without photons and that require collisions are common. For example, the exothermic chemical reaction of H + H to form H_2 does not occur with the emission of a photon. Rather, the reaction requires a collision with a third body, M, to remove the bond energy-H + H + M $\rightarrow$ H_2 + M* [12]. The third body distributes the energy from the exothermic reaction, and the end result is the H_2 molecule and an increase in the temperature of the system. Some commercial phosphors are based on nonradiative energy transfer involving multipole coupling. For example, the strong absorption strength of Sb^{3+} ions along with the efficient nonradiative transfer of excitation from Sb^{3+} to Mn^{2+}, are responsible for the strong manganese luminescence from phosphors containing these ions [13]. Similarly, the $n = 1$ state of hydrogen and the $n = 1/\text{integer}$ states of hydrogen are nonradiative, but a transition between two nonradiative states is possible via a nonradiative energy transfer, say $n = 1$ to $\frac{1}{2}$. In these cases, during the transition the electron couples to another electron transition, electron transfer reaction, or inelastic scattering reaction which can absorb the exact amount of energy that must be removed from the hydrogen atom. Thus, a catalyst provides a net positive enthalpy of reaction of $m \times 27.2$ eV (i.e. it absorbs $m \times 27.2$ eV where m is an integer). Certain atoms or ions serve as catalysts which resonantly accept energy from hydrogen atoms and release the energy to the surroundings to effect electronic transitions to fractional quantum energy levels.

The catalysis of hydrogen involves the nonradiative transfer of energy from atomic hydrogen to a catalyst which may then release the transferred energy by radiative and nonradiative mechanisms. As a consequence of the nonradiative energy transfer, the hydrogen atom becomes unstable and emits further energy until it achieves a lower-energy nonradiative state having a principal energy level given by Eqs. (1) and (2).

1.1. Inorganic catalysts

A catalytic system is provided by the ionization of t electrons from an atom to a continuum energy level such that the sum of the ionization energies of the t electrons is approximately $m \times 27.2$ eV where m is an integer. One such catalytic system involves strontium. The first through the fifth ionization energies of strontium are 5.69484, 11.03013, 42.89, 57, and 71.6 eV, respectively [14]. The ionization reaction of Sr to Sr^{5+}, $(t = 5)$, then, has a net enthalpy of

reaction of 188.2 eV, which is equivalent to $m=7$ in Eq. (3).

$$188.2\ \text{eV} + \text{Sr}(m) + \text{H}\left[\frac{a_H}{p}\right] \rightarrow \text{Sr}^{5+} + 5e^- + \text{H}\left[\frac{a_H}{(p+7)}\right] + [(p+7)^2 - p^2] \times 13.6\ \text{eV}, \quad (5)$$

$$\text{Sr}^{5+} + 5e^- \rightarrow \text{Sr}(m) + 188.2\ \text{eV}. \quad (6)$$

The overall reaction is

$$\text{H}\left[\frac{a_H}{p}\right] \rightarrow \text{H}\left[\frac{a_H}{(p+7)}\right] + [(p+7)^2 - p^2] \times 13.6\ \text{eV}. \quad (7)$$

The energy released during catalysis may undergo internal conversion and ionize or excite molecular and atomic hydrogen resulting in hydrogen emission which includes well-characterized ultraviolet lines such as the Lyman series. Lyman α emission was sought by EUV spectroscopy. Due to the extremely short wavelength of this radiation, "transparent" optics do not exist. Therefore, a windowless arrangement was used wherein the source was connected to the same vacuum vessel as the grating and detectors of the EUV spectrometer. Windowless EUV spectroscopy was performed with an extreme ultraviolet spectrometer that was mated with the cell. Differential pumping permitted a high pressure in the cell as compared to that in the spectrometer. This was achieved by pumping on the cell outlet and pumping on the grating side of the collimator that served as a pin-hole inlet to the optics. The cell was operated under hydrogen flow conditions while maintaining a constant hydrogen pressure in the cell with a mass flow controller.

The energy released during catalysis may also undergo internal conversion and ionize or excite molecular and atomic hydrogen and the catalysts resulting in visible emission. A cylindrical nickel mesh hydrogen dissociator of a gas cell also served as an electrode to produce a concentrically uniform radial electric field between the dissociator and the wall of the cylindrical stainless steel gas cell. Power was applied to the electrode to achieve a bright plasma which was recorded over the wavelength range $250\ \text{nm} \leqslant \lambda \leqslant 750$ nm. The power balance of a gas cell having atomized hydrogen and strontium was measured by integrating the total light output corrected for spectrometer system response and energy over the visible range. A control cell was identical except that sodium replaced strontium. In this case, 4000 times the power of the strontium cell was required in order to achieve the same optically measured light output power. A plasma formed at a cell voltage of about 250 V in the cell with hydrogen alone and in the cell with hydrogen and sodium; whereas, a plasma formed in the strontium cell at the extremely low voltage of about 2 V.

2. Experimental

2.1. EUV spectroscopy

The experimental set up shown in Fig. 1 comprised a quartz cell which was 500 mm in length and 50 mm in diameter. A sample reservoir that was heated independently using an external heater powered by a constant power supply was on one end of the quartz cell. Three ports for gas inlet, outlet, and photon detection were on the other end of the cell. A tungsten filament (0.5 mm, total resistance $\sim 2.5\ \Omega$) and a titanium cylindrical screen (300 mm long and 40 mm in diameter) that performed as a hydrogen dissociator were inside the quartz cell. A new dissociator was used for each experiment. The filament was 0.508 millimeters in diameter and 800 cm in length. The filament was coiled on a grooved ceramic support to maintain its shape when heated. The return lead ran through the middle of the ceramic support. The titanium screen was electrically floated. The power was applied to the filament by a Sorensen 80[illegible] power supply which was controlled by a constant power controller. The temperature of the tungsten filament was estimated to be in the range of 1100 to 1500°C. The external cell wall temperature was about 700°C. The hydrogen gas pressure inside the cell was maintained at about 300 mtorr with a hydrogen flow rate of 5.5 sccm controlled by a MKS 1179A21CS1BB 20 sccm range mass flow controller with a MKS type 246 readout. The entire quartz cell was enclosed inside an insulation package comprised of Zircar AL-30 insulation. Several K-type thermocouples were placed in the insulation to measure the key temperatures of the cell and insulation. The thermocouples were read with a multichannel computer data acquisition system.

In the present study, the light emission phenomena was studied for hydrogen, argon, neon, and helium alone; hydrogen with strontium, magnesium, barium, and sodium metals, and strontium alone. The pure elements of magnesium, barium, and strontium were placed in the reservoir and volatized by the external heater. Magnesium with a low vapor pressure (higher melting point) was volatilized by suspending a foil of the material (2 cm × 2 cm × 0.1 cm thick) between the filament and a titanium dissociator and heating the test material with the filament. The power applied to the filament was 300 W in the case of strontium and up to 600 W in the case of magnesium, barium, and sodium metals. The voltage across the filament was about 55 V and the current was about 5.5 A at 300 W. For the controls, magnesium, barium, and sodium metals, the cell was increased in temperature to the maximum permissible with the power supply.

The light emission was introduced to an EUV spectrometer for spectral measurement. The spectrometer was a McPherson 0.2 m monochromator (Model 302, Seya-Namioka type) equipped with a 1200 lines/mm holographic grating. The wavelength region covered by the monochromator was 30–560 nm. A channel electron multiplier (CEM) was used to detect the EUV light. The

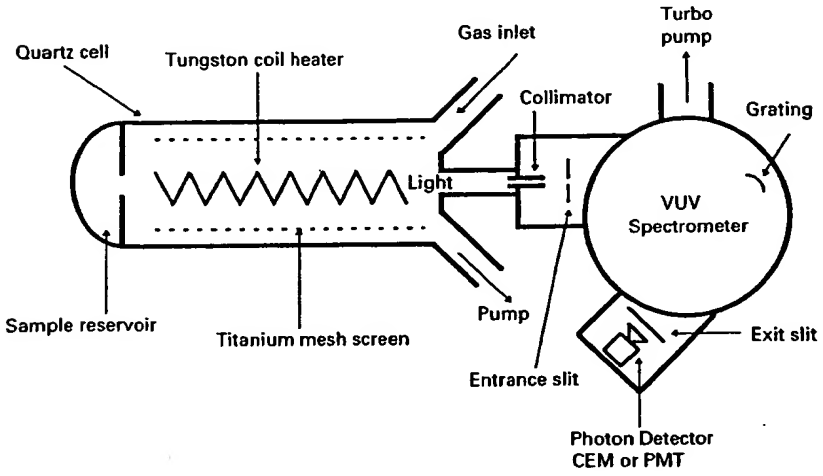

Fig. 1. The experimental set up comprising a gas cell light source and an EUV spectrometer which was differentially pumped.

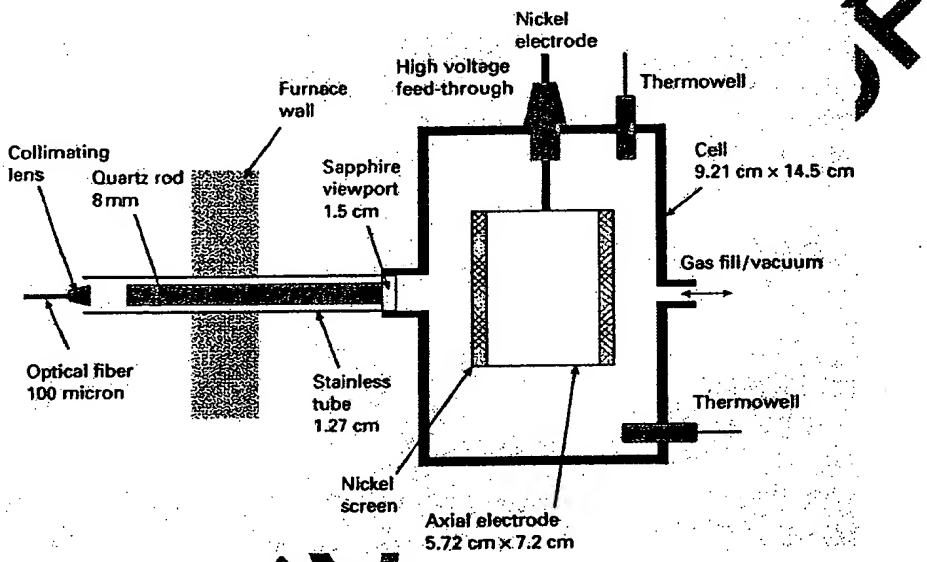

Fig. 2. Cylindrical stainless-steel gas cell for plasma studies with hydrogen alone, or with hydrogen with strontium or sodium.

wavelength resolution was about 12 nm (FWHM) with an entrance and exit slit width of 300 × 300 μm. The vacuum inside the monochromator was maintained below 5×10^{-4} torr by a turbo pump. The EUV spectrum (40–160 nm) of the cell emission with strontium present was recorded at about the point of the maximum Lyman α emission.

The UV/VIS spectrum (200–560 nm) of the cell emission with hydrogen alone was recorded with a photomultiplier tube (PMT) and a sodium salicylate scintillator. The PMT (Model R2687P Hamamatsu) used has a spectral response in the range of 185–680 nm with a peak efficiency at about 400 nm. The scan interval was 0.4 nm. The inlet and outlet slit were 500–500 μm.

The UV/VIS emission from the gas cell was channeled into the UV/VIS spectrometer using a 4 m long, five stand fiber optic cable (Edmund Scientific Model #E2549) having a core diameter of 1958 μm and a maximum attenuation of 0.19 dB/m. The fiber optic cable was placed on the outside surface of the top of the Pyrex cap of the gas cell. The fiber was oriented to maximize the collection of light emitted from inside the cell. The room was made dark. The other end of the fiber optic cable was fixed in an aperture manifold that attached to the entrance aperture of the UV/VIS spectrometer.

2.2. Power cell apparatus and procedure

Plasma studies with hydrogen alone or hydrogen with strontium or sodium were carried out in the cylindrical stainless-steel gas cell shown in Fig. 2. The experimental

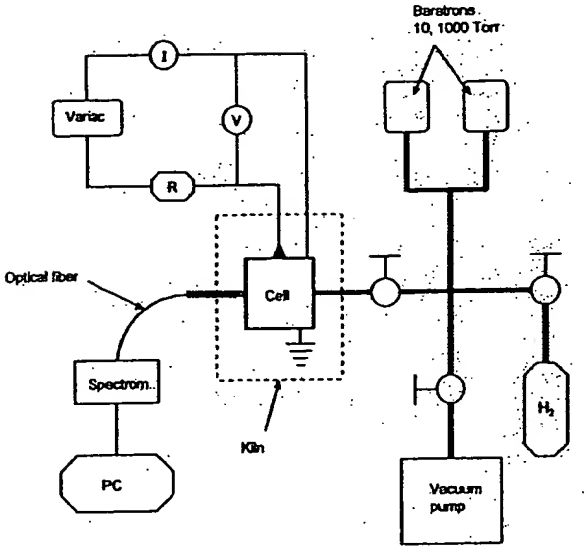

Fig. 3. The experimental setup for generating a glow discharge hydrogen plasma and for optically measuring the power balance.

setup for generating a glow discharge hydrogen plasma and for optically measuring the power balance is shown in Fig. 3. The cell was heated in a 10 kW refractory brick kiln (L & L Kiln Model JD230) as shown in Fig. 3. The kiln had three heating zones and a heated floor that were each heated by separate radiant elements. The zone temperatures were independently controlled by a Dynatrol controller using the temperatures read by 3 type-K thermocouples located adjacent to the kiln inner wall. The cell was evacuated and pressurized with hydrogen through a single 0.95 cm feed through. The discharge was started and maintained by an alternating current electric field in the 1.75 cm annular gap between an axial electrode and the cell wall. The cylindrical cell was 9.21 cm in diameter and 14.5 cm in height. The axial electrode was a 5.08 cm OD by 7.2 cm long stainless steel tube wound with several layers of nickel screen. The overall diameter of the axial electrode was [illegible] cm. A 1.6 mm thick UV-grade sapphire window with 1.5 cm view diameter provided a visible light path from inside the cell. The viewing direction was normal to the cell axis. A 1.27 cm diameter stainless steel tube passed through the furnace wall and connected to a view port welded to the cell wall at mid-height to provide an optical light path from the sapphire window to the furnace exterior. An 8 mm quartz rod channeled the light from the view port through the stainless steel tube to a collimating lens which was focused on a 100 μm optical fiber located outside the furnace. Spectral data were recorded with a visible spectrometer (Ocean Optics S2000) and stored by a personal computer.

The field voltage was controlled by a variable voltage transformer operating from 115 VAC, 60 Hz. A step-up transformer was used when necessary. True rms voltage at the axial electrode was monitored by a digital multimeter (Fluke 8010 A or Tenma 726202). A second multimeter (Extech 380763) in series with the discharge gap was used to indicate the current. The cell temperature was measured by a thermocouple probe located in the cell interior approximately 2 cm from the discharge gap. The pressure in the hydrogen supply tube outside the furnace was monitored by 10 and 1000 torr MKS Baratron absolute pressure gauges. In the absence of hydrogen flow, the hydrogen supply tube pressure was essentially the cell hydrogen partial pressure.

Strontium (Aldrich Chemical Company 99.9%) or sodium (Aldrich Chemical Company 99.95%) metals were loaded into the cell under a dry argon atmosphere. The cell was evacuated with a turbo vacuum pump to a pressure of 4 mtorr during most of the heating process. During the heat-up the cell was periodically pressurized with hydrogen (99.999% purity) to approximately [illegible] torr and subsequently evacuated to purge gaseous contaminants from the system. When the cell temperature stabilized, hydrogen was added until the steady pressure was approximately 1 torr. The field voltage was increased until breakdown occurred which was confirmed by the spectrometer response to visible light emitted from the cell. The hydrogen pressure was adjusted as much as possible to maximize the light emission from the cell. The voltage was maintained at the minimum level which resulted in a stable discharge during data acquisition.

Glow discharges were formed in pure control gases to determine their behavior as function of temperature and pressure. For He, N_2, and H_2 gases, the starting voltage to form a glow discharge, the voltage to maintain the discharge, and the light emitted were studied as a function of pressure at [illegible] and 662°C. The discharged was formed in the cylindrical stainless-steel gas cell used for plasma studies with hydrogen alone, or with hydrogen with strontium or sodium as shown in Fig. 2. The experimental setup was identical to that used for generating a glow discharge hydrogen plasma and for optically measuring the power balance as shown in Fig. 3. The methods for forming a glow discharge and the procedure for measuring the voltage and current were as given previously. The presence or absence of light emission was observed visually.

After thorough evacuation, the cell was filled to the desired pressure with test gas. The electrode voltage was gradually increased until a rush of current (at least 3 mA) was observed in the circuit. The greatest voltage for which no current flowed was recorded as the starting voltage V_s. Once a discharge was present, the electrode voltage was slowly decreased until the current abruptly fell to zero. The lowest voltage for which current persisted was recorded as the maintenance voltage. Light emission from the discharge, if present, was noted. The results are given in the appendix.

Table 1
Reference source calibration data for Ocean Optics S2000 Spectrometer

λ (nm)	$G_{\lambda r}$ ($\mu W/cm^2$ nm)	λ (nm)	$G_{\lambda r}$ ($\mu W/cm^2$ nm)	λ (nm)	$G_{\lambda r}$ ($\mu W/cm^2$ nm)
300	0.0036	400	0.0194	650	0.502
310	0.0023	420	0.031	700	0.697
320	0.0020	440	0.046	750	0.969
330	0.0021	460	0.065	800	1.344
340	0.0028	480	0.090	850	1.914
350	0.0039	500	0.118	900	2.742
360	0.0057	525	0.162	950	3.798
370	0.0082	550	0.214	1000	4.973
380	0.0113	575	0.274	1050	6.110
390	0.0148	600	0.342		

2.3. Spectrometer calibration for optical power balance measurement

Only a small portion of the light emission from the source was incident upon the spectrometer CCD detector since irradiation of the detector was dependent upon optical losses between the source and detector. The light of a small solid angle (1) passed through the sapphire window, (2) entered the quartz rod, (3) was channeled from the view port through the stainless-steel tube to the collimating lens, (4) was focused on the 100 μm optical fiber, (5) was carried on the optical fiber, (6) entered the spectrometer, and (7) ultimately was incident on the CCD detector. Attenuation occurred at each interface and along each optical element. To standardize these factors for the emission of strontium vapor with hydrogen, the control experiments of hydrogen alone and sodium vapor with hydrogen were run under identical conditions. Thus, these experiments served as standard light sources. However, the spectra of each experiment was unique. The spectrometer system comprised the 100 μm optical fiber and the visible spectrometer (Ocean Optics S2000). To correct for the nonuniform response of the spectrometer system as a function of wavelength and the dependence of energy on wavelength, the system was calibrated against a reference light source.

During the recording of each spectrum, the spectrometer integration time was adjusted to maximize its sensitivity as recommended by the manufacturer (Ocean Optics). The recorded intensity versus wavelength was a rate; thus, it was independent of the integration time. And, all spectra were comparable since they were acquired such that the spectrometer was operating in a linear response range.

The spectral irradiation of the spectrometer system G_λ (energy/time-area-wavelength) was the rate at which energy in the wavelength interval $\lambda - \lambda + d\lambda$ was incident on the fiber optic entrance of the spectrometer system per unit area and per unit wavelength interval $d\lambda$. The corresponding spectrometer response or count rate S_λ (counts/s) was

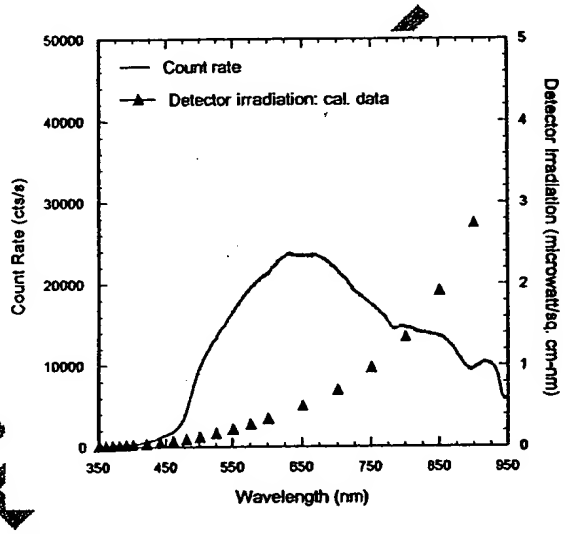

Fig. 4. The plot of the reference source count rate $S_{\lambda r}$ and the calibration data $G_{\lambda r}$.

proportional to spectrometer system irradiation,

$$S_\lambda = b_\lambda G_\lambda. \tag{8}$$

The spectral dependence of the proportionality factor b_λ arises from spectral bias of the spectrometer system. The radiant flux input to the spectrometer system was obtained by calibration with a reference light source (Ocean Optics LS-1-CAL) for which the radiant flux was known. The distribution of the spectrometer system irradiation by the reference light source $G_{\lambda r}(\lambda)$ was supplied in tabular form by Ocean Optics as given in Table 1. The count rate due to irradiation by the reference source was

$$S_{\lambda r} = b_\lambda G_{\lambda r}, \tag{9}$$

where $G_{\lambda r}$ is the spectrometer system irradiation by the reference light source. Then the spectrometer system

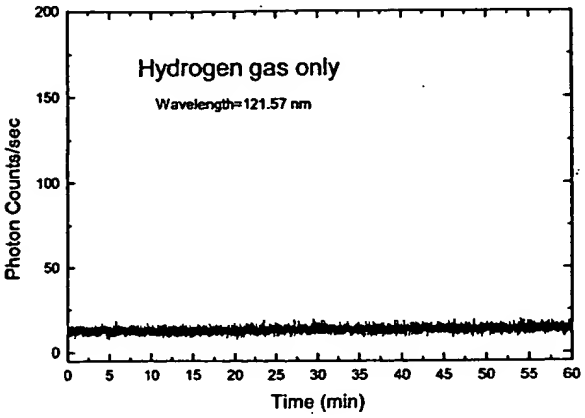

Fig. 5. The intensity of the Lyman α emission as a function of time from the gas cell at a cell temperature of 700°C comprising a tungsten filament, a titanium dissociator, and 300 mtorr hydrogen with a flow rate of 5.5 sccm.

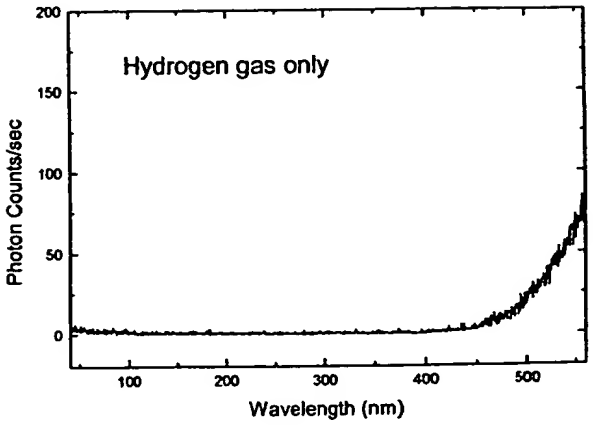

Fig. 6. The UV/VIS spectrum (40–560 nm) of the cell emission from the gas cell at a cell temperature of 700°C comprising a tungsten filament, a titanium dissociator, and 300 mtorr hydrogen with a flow rate of 5.5 sccm that was recorded with a photomultiplier tube (PMT) and a sodium salicylate scintillator.

irradiation by the source under study was given by

$$G_\lambda = S_\lambda \frac{G_{\lambda r}}{S_{\lambda r}}. \tag{10}$$

The ratio

$$\frac{G_{\lambda r}}{S_{\lambda r}} = \left[\frac{\mu W/cm^2\ nm}{cts/s}\right] \tag{11}$$

was the spectral calibration factor for the system. This calibration approach holds regardless of whether the count rate is proportional to radiant energy/time or photons/time. In the latter case the proportionality factor b_λ accounts for the spectral bias of the photons as well as the spectral bias of the spectrometer system (i.e. b_λ includes the factor $(h\nu)^{-1}$). The reference source count rate $S_{\lambda r}$ and the calibration data $G_{\lambda r}$ are plotted in Fig. 4. The spectral bias of the system which favored mid-range wavelengths (550–750 nm) is clear. Manual calibration of the raw count rate data was carried out using calibration Eq. (10) for the hydrogen–strontium mixture and background radiation tests. In the remaining cases, the calibration was done in real time by the Ocean Optics spectrometer software OOIrad. The total visible radiant flux incident on the spectrometer system was given by

$$G = \int_{\lambda=400\ nm}^{\lambda=700\ nm} G_\lambda(\lambda)\, d\lambda, \tag{12}$$

where $G_\lambda(\lambda)$ is the spectral irradiation. G_λ, S_λ, and G were each a rate, thus, they were independent of the integration time.

3. Results

3.1. EUV Spectroscopy

The cell without any test material present was run to establish the baseline of the spectrometer. The intensity of the

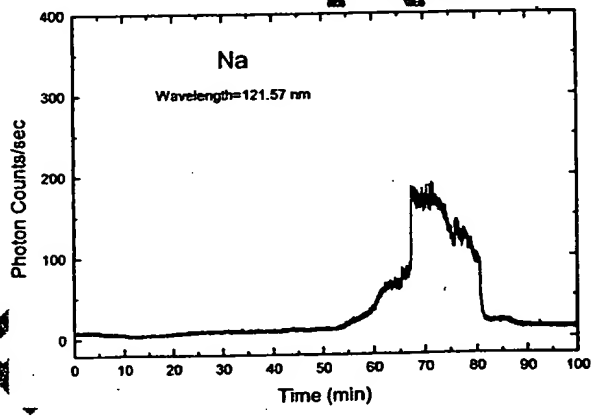

Fig. 7. The intensity of the Lyman α emission as a function of time from the gas cell at a cell temperature of 700°C comprising a tungsten filament, a titanium dissociator, sodium metal vaporized from the catalyst reservoir, and 300 mtorr hydrogen with a flow rate of 5.5 sccm.

Lyman α emission as a function of time from the gas cell at a cell temperature of 700°C comprising a tungsten filament, a titanium dissociator, and 300 mtorr hydrogen with a flow rate of 5.5 sccm is shown in Fig. 5. The UV/VIS spectrum (40–560 nm) of the emission from the gas cell at a cell temperature of 700°C comprising a tungsten filament, a titanium dissociator, and 300 mtorr hydrogen with a flow rate of 5.5 sccm is shown in Fig. 6. The spectrum was recorded with a photomultiplier tube (PMT) and a sodium salicylate scintillator. No emission was observed except for the blackbody filament radiation at the longer wavelengths. No emission was also observed when argon, neon, or helium replaced hydrogen.

The intensity of the Lyman α emission as a function of time from the gas cell at a cell temperature of 700°C com-

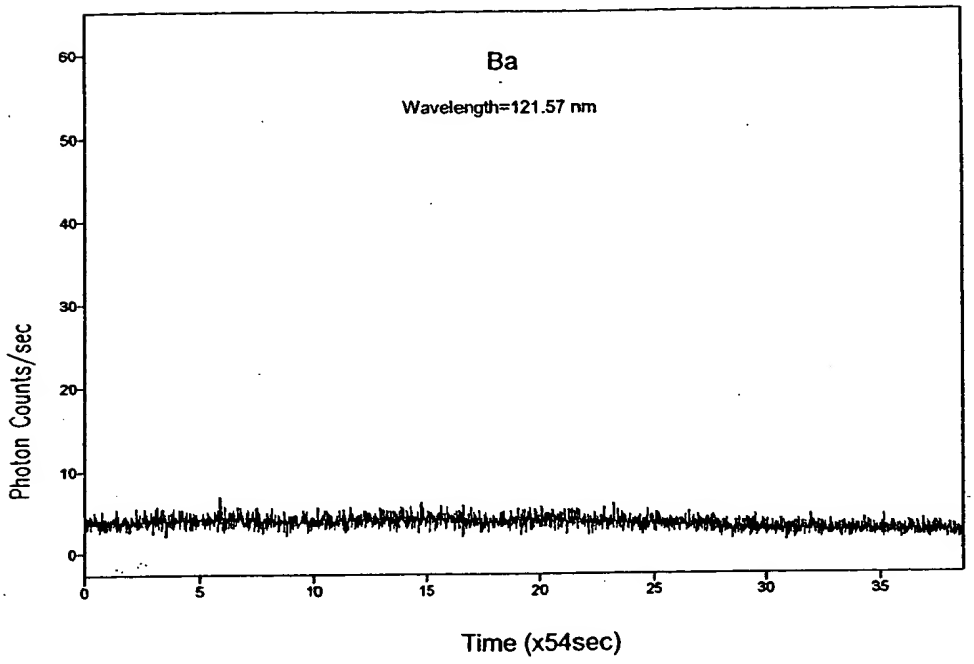

Fig. 8. The intensity of the Lyman α emission as a function of time from the gas cell at a cell temperature of 700°C comprising a tungsten filament, a titanium dissociator, barium metal vaporized from the catalyst reservoir, and 300 mtorr hydrogen with a flow rate of 5.5 sccm.

prising a tungsten filament, a titanium dissociator, sodium or barium metal in the catalyst reservoir, and 300 mtorr hydrogen with a flow rate of 5.5 sccm are shown in Figs. 7 and 8, respectively. Sodium or barium metal was volatized from the catalyst reservoir by heating it with an external heater. No emission was observed in either case. The maximum filament power was over 500 W. A metal coating formed in the cap of the cell over the course of the experiment in both cases.

The intensity of the Lyman α emission as a function of time from the gas cell at a cell temperature of 700°C comprising a tungsten filament, a titanium dissociator, a magnesium foil in the cell, and strontium metal in the catalyst reservoir, and 300 mtorr hydrogen with a flow rate of 5.5 sccm are shown in Figs. 9 and 10, respectively. The magnesium foil was volatilized by suspending a 2 cm × 2 cm × 0.1 mm thick foil between the filament and the titanium dissociator and heating the foil with the filament. Emission was observed with the magnesium foil and hydrogen. The maximum filament power was 500 W. The temperature of the foil increased with filament power. At 500 W, the temperature of the foil was 1000°C which would correspond to a vapor pressure of about 100 mtorr. Strontium metal was volatized from the catalyst reservoir by heating it with an external heater. Strong emission was observed from strontium and hydrogen. The EUV spectrum (40–160 nm) of the cell emission recorded at about the point of the maximum Lyman α emission is shown in Fig. 11. No emission was observed when hydrogen was stopped. A metal coating formed in the cap of the cell over the course of the experiment in the case of magnesium and strontium.

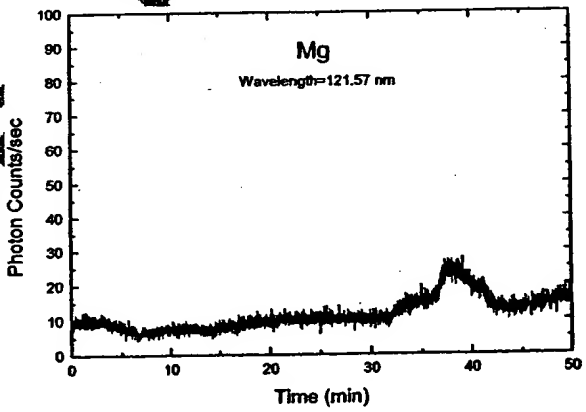

Fig. 9. The intensity of the Lyman α emission as a function of time from the gas cell at a cell temperature of 700°C comprising a tungsten filament, a titanium dissociator, a magnesium foil, and 300 mtorr hydrogen with a flow rate of 5.5 sccm.

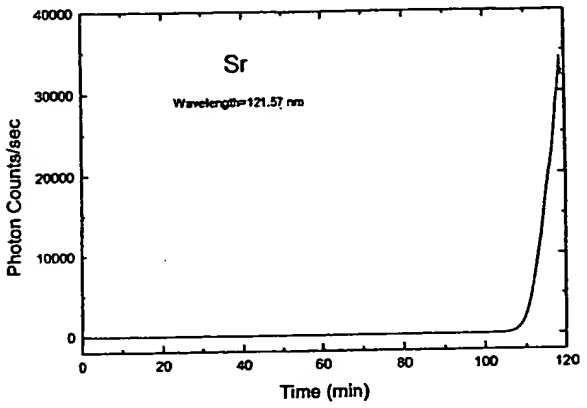

Fig. 10. The intensity of the Lyman α emission as a function of time from the gas cell at a cell temperature of 700°C comprising a tungsten filament, a titanium dissociator, strontium metal vaporized from the catalyst reservoir, and 300 mtorr hydrogen with a flow rate of 5.5 sccm.

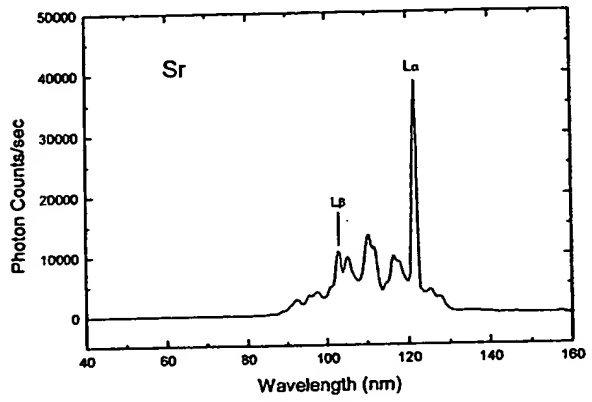

Fig. 11. The EUV spectrum (40–160 nm) of the cell emission recorded at about the point of the maximum Lyman α emission from the gas cell at a cell temperature of 700°C comprising a tungsten filament, a titanium dissociator, strontium metal vaporized from the catalyst reservoir, and 300 mtorr hydrogen with a flow rate of 5.5 sccm.

3.2. Optically measured power balance

Count rate and spectrometer system irradiation of the background spectrum of hydrogen and strontium vapor over the wavelength range $350 \leqslant \lambda \leqslant 750$ nm in the absence of power applied to the electrode and in the absence of a discharge is shown in Fig. 12. These data were collected during cell evacuation following the test with strontium and hydrogen at a cell temperature of 664°C. The maximum visible irradiation of 0.014 μW/cm² nm occurred at the red end of the visible spectrum. The total visible radiant flux incident on the spectrometer system over the visible range $400 \leqslant \lambda \leqslant 700$ nm was given by Eq. (12). The integral was approximated by rectangles with panel width $\Delta\lambda = 0.342$ nm. The results are summarized in Table 2 where T is the temperature, P_{hyd} is the hydrogen partial pressure, and P_v is the equilibrium metal vapor pressure calculated from standard curves of the vapor pressure as a function of temperature [15].

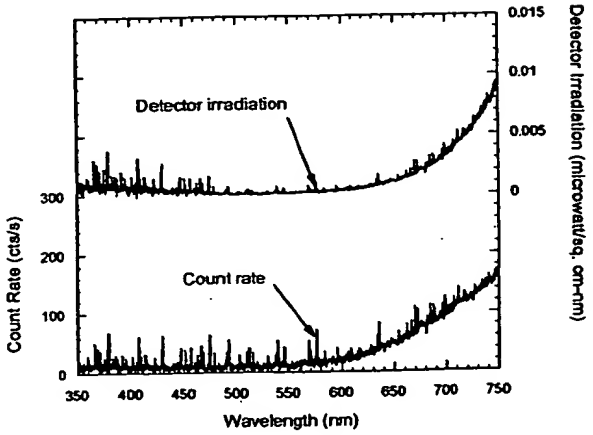

Fig. 12. Count rate and spectrometer system irradiation of the background spectrum of hydrogen and strontium vapor over the wavelength range $350 \leqslant \lambda \leqslant 750$ nm in the absence of power applied to the electrode and in the absence of a discharge.

Power was applied to the electrode to achieve a bright plasma in hydrogen alone and in hydrogen with strontium or sodium vapor for cell temperatures in the range 335–664°C. In each case, the spectral radiant flux at the spectrometer system was recorded. The power driving the hydrogen alone and hydrogen plus sodium vapor controls was adjusted such that the peak spectrometer system spectral radiation was about 0.1 μW/cm² nm in each case. The integrated visible irradiation levels (0.40 to 2.08 μW/cm²) were of the same order of magnitude despite the differences in frequencies of the spectral lines recorded by the spectrometer system in the strontium case versus the controls.

The power required to maintain a plasma of equivalent optical brightness with strontium atoms present was 4000 times less than that required for the controls. For example, a driving power of 33.7 W was necessary to achieve a total visible radiant flux of about 1 μW/cm² from a sodium hydrogen mixture; whereas, 8.5 mW formed a plasma with the same optical brightness in the case of a strontium hydrogen mixture. A plasma formed at a cell voltage of about 250 V in the cell with hydrogen alone and in the cell with hydrogen and sodium; whereas, a plasma formed in the strontium cell at the extremely low voltage of about 2 V. The results are summarized in Table 2.

The count rate and the spectrometer system irradiation for a mixture of strontium vapor and hydrogen at 664°C is shown in Fig. 13. Optimal light emission was observed after several hours of cell evacuation. The hydrogen partial pressure was unknown under these conditions. The calculated equilibrium vapor pressure of strontium at 664°C is approximately 270 mtorr. The measured breakdown volt-

Table 2
Discharge conditions and comparison of the driving power to achieve a total visible radiant flux of about 1 μW/cm²

	T (°C)	P_{hyd} (Torr)	P_v (Torr)[a]	Voltage (V)	Current (mA)	Integration Time[b] (ms)	G (μW/cm²)	Power (W)
H_2 + Sr	664	—	0.270	2.20	3.86	768	1.17	0.0085
H_2	664	1.0	—	224	110	1130	2.08	24.6
H_2 + Na	335	1.0	0.051	272	124	122	1.85	33.7
H_2 + Na	516	1.5	5.3	220	68	768	0.40	15.0
H_2 + Na	664	1.5	63	240	41	768	0.41	9.84
Bkgnd.	664	—	0.270	0	0	768	0.20	0

[a]Calculated [15].
[b]G is independent of the integration time since it is a rate.

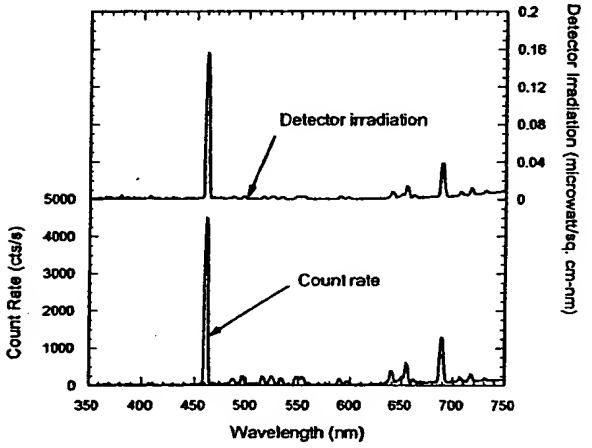

Fig. 13. The count rate and the spectrometer system irradiation for a mixture of strontium vapor and hydrogen at 664°C.

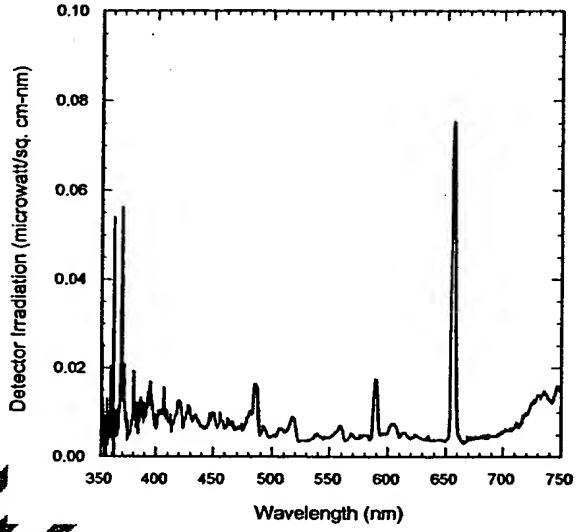

Fig. 14. The spectrometer system irradiation for a hydrogen discharge at a cell temperature of 664°C and a hydrogen pressure of 1 torr.

Table 3
Spectral features of hydrogen and strontium at 664°C

Measured wavelength (nm)	Spectrometer system irradiation (μW/cm² nm)	Published emission data [16] (nm)
460.6	0.156	460.73 (Sr)
487.2	0.00290	487.29 (Sr), 486.13 (H_2)
639.8	0.00813	639.92 (Sr)
654.7	0.0139	654.68 (Sr), 656.29 (H_2)
689.4	0.0386	689.26 (Sr)

age was approximately 2 V. The maintenance voltage for a stable discharge was 2.2 V and input power was 8.5 mW. Spectral characteristics are noted in Table 3. The hydrogen Balmer α and β peaks were obscured by strong strontium emission near 654.7 and 487.2 nm, respectively.

The spectrometer system irradiation for a hydrogen discharge at a cell temperature of 664°C and 1 torr is shown in Fig. 14. The breakdown voltage was approximately 220 V. The field voltage required to form a stable discharge was 224 V. The input power was 24.6 W. Spectral features are tabulated in Table 4. The peak at 589.1 nm may be due to sodium contamination from a previous experimental run. The minor peaks at 518.2 and 558.7 nm have not been identified.

The spectrometer system irradiation for mixtures of sodium vapor and hydrogen are shown in Figs. 15–17 for temperatures of 335, 516, and 664°C, respectively. Corresponding hydrogen pressures are 1, 1.5, and 1.5 torr, respectively. The calculated sodium vapor pressure was 51 mtorr, 5.3 torr, and 63 torr at 335, 516, and 664°C, respectively. At least 200 V was required to maintain a discharge. The input power for a stable discharge ranged from approximately 10 W at 664°C to 34 W at 335°C. Spectral features corresponding to 335°C are summarized in Table 5. Strong emission observed near

Table 4
Spectral features of hydrogen at 664°C

Measured wavelength (nm)	Spectrometer system irradiation ($\mu W/cm^2$ nm)	Published emission data [16] (nm)
485.8	0.0165	486.13 (H_2)
518.2	0.00894	
558.7	0.00694	
589.1	0.0174	589.00 (Na), 589.59 (Na)
656.7	0.0752	656.29 (H_2)

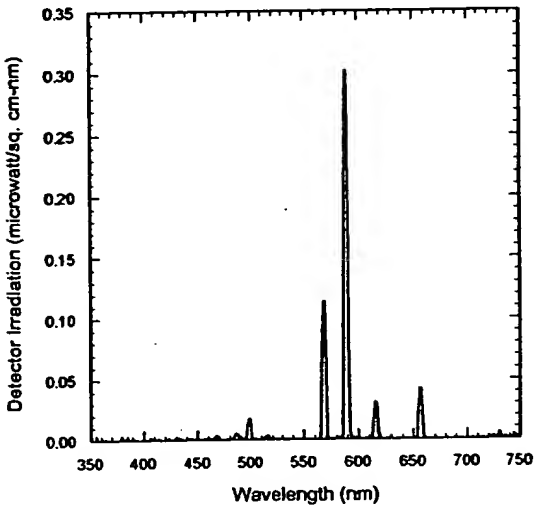

Fig. 15. The spectrometer system irradiation for a mixture of sodium vapor and hydrogen at 335°C.

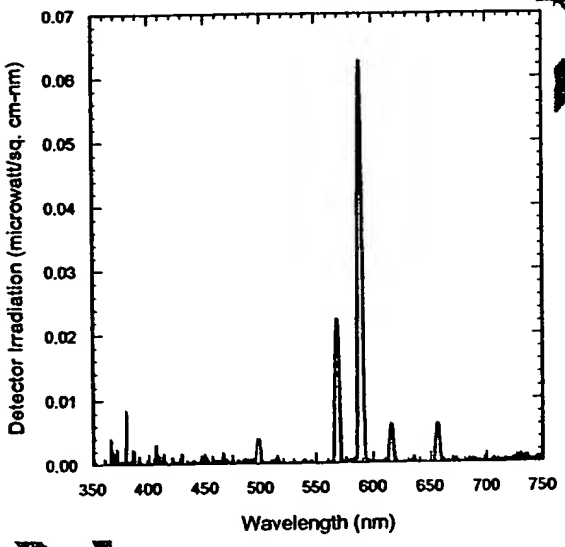

Fig. 16. The spectrometer system irradiation for a mixture of sodium vapor and hydrogen at 516°C.

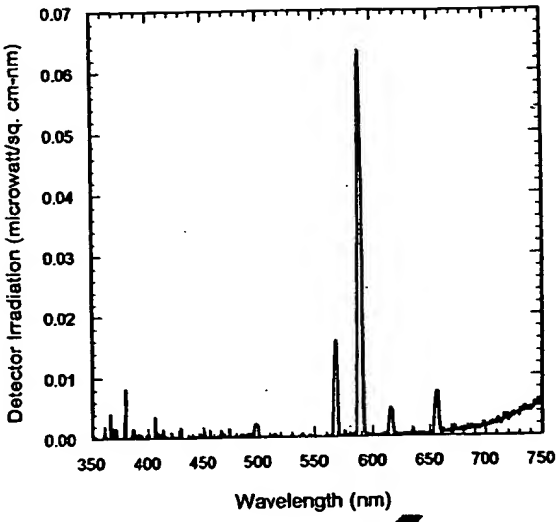

Fig. 17. The spectrometer system irradiation for a mixture of sodium vapor and hydrogen at 664°C.

Table 5
Spectral features of hydrogen and sodium at 335°C

Measured wavelength (nm)	Spectrometer system irradiation ($\mu W/cm^2$ nm)	Published emission data [16] (nm)
467.[illegible]	0.00400	466.86 (Na)
48[illegible]	0.0055	486.13 (H_2)
498.4	0.0176	498.28 (Na)
[illegible].1	0.00380	515.34 (Na)
[illegible].[illegible]	0.114	568.82 (Na)
[illegible].3	0.302	589.00 (Na), 589.59 (Na)
615.9	0.0310	616.07 (Na)
656.0	0.0422	656.29 (H_2), 655.24 (Na)
657.0	0.0421	656.29 (H_2)

656–657 nm was probably due, in-part, to hydrogen. The relative contribution to the intensity was masked by strong sodium emission at a slightly shorter wavelength. The peak at 486.2 nm could only be due to hydrogen emission. Sodium does not have emission lines in the neighborhood of this wavelength. The intensity of this peak diminishes relative to the more prominent sodium peaks with increasing temperature as shown in Figs. 15–17. This may have been due to a decreasing hydrogen concentration as the sodium vapor pressure increased.

The minimum starting voltage $V_{s\,min}$ determined with a variation of the discharge gas pressure and the corresponding pressure of the discharge gas defined as P_{min} are given in Table 6. The minimum voltage required to form a plasma in hydrogen at 662°C was about 200 V. Gas parameters from von Engel [17] and Naidu and Kamaraju [18] shown

Table 6
The minimum starting voltage $V_{s\,min}$ determined with a variation of the discharge gas pressure and the corresponding pressure of the discharge gas defined as P_{min}

	25°C		662°C	
Gas	$V_{s\,min}$ (V)	P_{min} (torr)	$V_{s\,min}$ (V)	P_{min} (torr)
He	162	2.20	145	7.37
N_2	212	0.417	180	1.35
H_2	185	0.70	195	2.44

in Table 7 indicate a minimum voltage of 273 V is required at 25°C. Further results of the behavior of glow discharges in control gases as a function of pressure and temperature are given in the appendix.

4. Discussion

In the cases where Lyman α emission was observed, no possible chemical reactions of the tungsten filament, the dissociator, the vaporized test material, and 300 mtorr hydrogen at a cell temperature of 700°C could be found which accounted for the hydrogen α line emission. In fact, no known chemical reaction releases enough energy to excite Lyman α emission from hydrogen. The emission was not observed with hydrogen alone or with helium, neon, or argon gas. Intense emission was observed for strontium with hydrogen gas, but no emission was observed with hydrogen or strontium alone. This result indicates that the emission was due to a reaction of hydrogen. The emission of the Lyman lines is assigned to the catalysis of hydrogen which excites atomic and molecular hydrogen. Other studies support the possibility of a novel catalytic reaction of atomic hydrogen. It has been reported that intense extreme ultraviolet (EUV) emission was observed at low temperatures (e.g. $\approx 10^3$ K) from atomic hydrogen and certain atomized elements or certain gaseous ions [1–5]. The only pure elements that were observed to emit EUV were each a catalytic system wherein the ionization of t electrons from an atom to a continuum energy level is such that the sum of the ionization energies of the t electrons is approximately $m \times 27.2$ eV where t and m each are an integer. Strontium atoms ionize at integer multiples of the potential energy of atomic hydrogen and caused emission; whereas, the chemically similar atoms, magnesium and barium as well as sodium, caused no emission. The catalytic reactions for strontium are given by Eqs. (5)–(7). Whereas the enthalpy of ionization of Sr to Sr^{5+}, $m = 5$, then, has a net enthalpy of reaction of 188.2 eV which is equivalent to $m = 7$ in Eq. (3).

The power balance of a gas cell having atomized hydrogen and strontium was measured by integrating the total light output corrected for spectrometer system response and energy over the visible range. A control cell was identical except that sodium replaced strontium. In this case, 4000 times the power of the strontium cell was required in order to achieve that same optically measured light output power. A plasma formed at a cell voltage of about 250 V in the cell with hydrogen alone and in the cell with hydrogen and sodium; whereas, a plasma formed in the strontium cell at the extremely low voltage of about 2 V. The starting and maintenance discharge voltages were two orders of magnitude of that predicted by current theory or observed experimentally as shown in the appendix.

In the case of a potassium catalyst, a plasma was observed when the electric field was set to zero [4,5]. During the strontium catalysis reaction is given by Eqs. (5)–(7), the electrons are ionized to a continuum energy level. The presence of a low-strength electric field alters the continuum energy levels. The electric field in this experiment was about 2 V over the annular gap of about 2 cm. A weak field may adjust the energy of the ionizing strontium catalyst to match the energy released by hydrogen to cause it to undergo catalysis to the lower-energy state. In other words, the electric field may cause an energy resonance of the net enthalpies of reaction of strontium and hydrogen to permit the catalysis reaction.

5. Conclusions

Intense EUV emission was observed at low temperatures (e.g. $\approx 10^3$ K) from atomic hydrogen and strontium which ionizes at integer multiples of the potential energy of atomic hydrogen. The release of energy from hydrogen by the catalysis reaction with strontium atoms was evidenced by the EUV emission and by the formation of an optically bright plasma with 4000 times less input power and 2% of the voltage of that required to form an equivalent plasma with sodium and hydrogen. The energy release must result in a lower-energy state of hydrogen. The lower-energy hydrogen atom called a hydrino atom by Mills [11] would be expected to demonstrate novel chemistry. The formation of novel compounds based on hydrino atoms would be substantial evidence supporting catalysis of hydrogen as the mechanism of the observed EUV emission. A novel hydride ion called a hydrino hydride ion having extraordinary chemical properties given by Mills [11] is predicted to form by the reaction of an electron with a hydrino atom. Compounds containing hydrino hydride ions have been isolated as products of the reaction of atomic hydrogen with atoms and ions identified as catalysts in the present EUV study [1–5,11, 19–24].

Billions of dollars have been spent to harness the energy of hydrogen through fusion using plasmas created and heated to extreme temperatures by RF coupling (e.g. $> 10^6$ K) with confinement provided by a toroidal magnetic field. The present study indicates that energy may be released from hydrogen at relatively low temperatures with an apparatus

Table 7
Gas parameters from von Engel [17] and Naidu and Kamaraju [18]

Gas	A (cm^{-1} $torr^{-1}$)	B (V/cm torr)	X/P (V/cm torr)	$V_{s\,min}$ (V)	$(Pd)_{min}$ (cm torr)	β
N_2	12	342	100–600	251	0.67	3.24
H_2	5.4	139	20–1000	273	1.15	3.90
Air	15	365	100–800	327	0.567	4.94
CO_2	20	466	500–1000	420	0.51	6.63
Ar	12	180	100–600	137	0.9	3.36
He	3	34	20–150	156	4.0	5.06
Hg	20	370	200–600	520	2	10.3
Na	—	—	—	335	0.04	—

which is of trivial technological complexity compared to a tokomak. And, rather than producing radioactive waste, the reaction has the potential to produce compounds having extraordinary properties. The implications are that a vast new energy source and a new field of hydrogen chemistry have been discovered. Work in progress includes synthesis and identification of novel compounds, spectroscopy of the plasma producing process, and energy balance measurements.

Acknowledgements

Special thanks are due to Nelson Greenig for designing the fiber optic system, to Jinquan Dong for preparing many of the cells comprising the test materials, to Takeyoshi Onuma for recording EUV and optical spectra and to Bala Dhandapani and Jiliang He for reviewing this manuscript.

Appendix A. Electrical breakdown and discharge processes

A.1. Summary of results

For He, N_2, and H_2 gases, the starting voltage to form a glow discharge, the voltage to maintain the discharge, and the light emitted were studied as a function of pressure at 25 and 662°C. A summary of the observations follows:

1. The starting voltage exhibited a minimum with respect to the variation in pressure as predicted by Townsend theory. The minimum starting voltage, $V_{s\,min}$, occurred at a pressure defined as P_{min} shown in Table 6.
2. For helium, the minimum starting voltage was lower, and P_{min} was higher than that observed for N_2 and H_2.
3. For helium and nitrogen, $V_{s\,min}$ decreases by less than 16% when the temperature was increased from 25 to 662°C. For H_2, $V_{s\,min}$ is almost independent of temperature.
4. For He, N_2, and H_2 gases at 25°C, the measured values of the pressure-electrode gap spacing product corresponding to $V_{s\,min}$, $(Pd)_{min}$, are in good agreement with published values.
5. For He, N_2, and H_2 gases, P_{min} shifts toward higher pressure with increasing temperature. For a given gas, P_{min} occurs at approximately the same gas number density for 25 and 662°C, in agreement with theory.
6. At room temperature, Townsend theory was a fair predictor of the starting voltage for N_2 and H_2 and a good predictor of P_{min} for He and N_2.
7. For He, N_2, and H_2 gases, a glow discharge was observed for a range of pressures about P_{min}. Light emission was greatest for pressures very near P_{min}. For pressures substantially greater than or substantially less than P_{min}, a discharge was formed (conducting gas) with little or no light emission.
8. No net H_2 are consumed when a discharge was present at 662°C. This may result from nitride and hydride formation during the discharge.

A.2. Theoretical background

Consider a gas layer of thickness d bounded by plane electrodes. The gas pressure is P and the electrode potential is V. Electrons are periodically released from the cathode, perhaps due to ultraviolet irradiation, by cosmic radiation, etc. These primary electrons constitute a small current i_0. The primary electrons experience numerous collisions as they accelerate toward the anode in the electric field. Two important types of collision, corresponding to ionization and excitation, are

$$e^- + N \rightarrow e^- + N^+ + e^-, \tag{A.1}$$

$$e^- + N \rightarrow e^- + N^*, \tag{A.2}$$

where e^-, N, N^* and N^+ represent an electron, a neutral particle, an excited neutral particle, and a positive ion, respectively. Let α be the number of positive ion/electron pairs produced by a primary electron per unit length in the field direction. α is Townsend's first ionization coefficient. Ignoring recombination and the formation of negative ions, electron multiplication results in the current

$$i = i_0 e^{\alpha d} \tag{A.3}$$

at the anode [17]. The current at the anode is balanced by positive ions reaching the cathode where they combine with electrons and return to the gas as neutral particles.

Electrons are also released from the cathode due to bombardment by positive ions and excited neutral particles, and due to irradiation by excited particles in the gap [25]. These secondary electrons are accelerated in the field and result in electron multiplication just as the primary electrons. Eq. (A.3) for i ignores these secondary electrons. For simplicity, assume that the secondary electrons are produced at the cathode by positive ion impact alone. Denote by γ the number of secondary electrons produced by a positive ion arriving at the cathode. Common gases and cathode materials result in $0.001 < \gamma < 0.1$, approximately. γ is Townsend's second ionization coefficient. The current at the anode including multiplication by secondary electrons is [17]

$$i = \frac{i_0 e^{ad}}{1 - \gamma(e^{ad} - 1)}. \tag{A.4}$$

In this equation for current growth, the ionization coefficients for a particular gas and cathode material at a fixed temperature are functions of the field strength

$$X = \frac{V}{d} \tag{A.5}$$

and the gas pressure. More precisely

$$\frac{\alpha}{P} = f_1\left(\frac{X}{P}\right), \tag{A.6}$$

$$\gamma = f_2\left(\frac{X}{P}\right). \tag{A.7}$$

The physical basis for these relationships follows from the relationship between the mean free path of an electron in the gas, λ_e, and the gas pressure

$$P \propto \frac{1}{\lambda_e} = \frac{\text{collisions}}{\text{distance traveled}} \propto \frac{\text{collisions}}{\text{distance traveled in field direction}}. \tag{A.8}$$

The second proportionality follows from the ratio of electron random velocity to drift velocity, v/v_d = constant [25]. The interpretations for α/P and X/P follow from the definitions of α and X:

$$\frac{\alpha}{P} = \propto \frac{\text{ionizations}}{\text{collision}}, \tag{A.9}$$

$$\frac{X}{P} = \propto \frac{\text{potential}}{\text{collision}} \tag{A.10}$$

For α/P, von Engel [17] develops a semi-empirical approximation

$$\frac{\alpha}{P} = Ae^{-B/(X/P)} \tag{A.11}$$

where A and B are constants. The approximation is valid for a limited range of the reduced field strength X/P, shown in Table 7.

The current growth (Eq. (A.4)) indicates that current multiplication in the gas is infinite when

$$\gamma(e^{ad} - 1) = 1. \tag{A.12}$$

This is the onset of breakdown. When this condition is reached the discharge becomes self-sustaining, requiring no flow of primary electrons from the cathode. Breakdown may occur for a fixed electrode spacing by increasing V. Introducing the functional expressions for the ionization coefficients and $X_s = V_s/d$ where V_s is the starting or breakdown voltage gives

$$f_2\left(\frac{V_s}{\text{Pd}}\right)\left(e^{(\text{Pd})f_1(V_s/\text{Pd})} - 1\right) = 1. \tag{A.13}$$

Therefore, the breakdown voltage is a function of the product of the pressure and the electrode spacing,

$$V_s = f(\text{Pd}). \tag{A.14}$$

The product Pd is directly proportional to the number of particles in the electrode gap as shown below. The breakdown voltage is the same for a gas at 10 torr between electrodes with 1 mm spacing as it is for the same gas at 1 torr between electrodes with 10 mm spacing. In each case, the number of particles in the gap is the same, and the potential for acceleration of an electron between successive collisions at breakdown is also the same for both cases.

From the ideal gas law, the gas number density is given by

$$n = \frac{PN_a}{RT} \tag{A.15}$$

where N_a is Avogadro's number, T is the absolute temperature, and R is the ideal gas constant. The number of particles between electrodes of unit area is

$$d\frac{PdN_a}{RT}. \tag{A.16}$$

Therefore, Pd is proportional to the number of particles between electrodes of unit area at a fixed temperature. Generalizing the functional relation (Eq. (A.14)) to account for temperature variations results in

$$V_s = \bar{f}(nd). \tag{A.17}$$

An approximation for the function f of Eq. (A.14) which ignores the temperature dependence is found by making the following substitutions into Eq. (A.13): (1) γ given by Eq. (A.7) where $X_s = V_s/d$ in Eq. (A.7) and the dependence of γ on X/P is ignored and (2) f_1 given by Eqs. (A.6) and (A.11) where $X_s = V_s/d$

$$\gamma[\exp\{A(\text{Pd})e^{-B/(X_s/P)}\} - 1] = 1. \tag{A.18}$$

Rearrangement leads to

$$\frac{X_s}{P} = \frac{B}{\log[A(\text{Pd})/\log(1 + 1/\gamma)]} \tag{A.19}$$

for the starting field strength or

$$V_s = \frac{B(\text{Pd})}{\log[A(\text{Pd})/\beta]}, \tag{A.20}$$

where

$$\beta = \log(1 + 1/\gamma). \tag{A.21}$$

This is Paschen's law for the breakdown voltage in a gas that holds approximately for Pd < 1000 cm · torr. Because $\log x$ varies more slowly than x for large x and more rapidly than x for small x, a minimum value of V_s is expected where

$$\frac{dV_s}{d(Pd)} = 0. \tag{A.22}$$

This minimum occurs for

$$Pd = (Pd)_{min} = \frac{e\beta}{A} \tag{A.23}$$

and has the value

$$V_{s\,min} = \frac{Be\beta}{A}. \tag{A.24}$$

The minimum in starting voltage occurs because Pd is proportional to the number of particles between the electrodes. For small Pd, few ionizations take place, and the electron multiplication is low due to the small number of particles in the gap. A large Pd results in closely spaced neutral particles so that few electrons acquire sufficient energy for ionization between collisions. Measured values of the minimum breakdown voltage and $(Pd)_{min}$ are given in Table 7 along with the estimate for β

$$\beta = \frac{AV_{s\,min}}{Be}. \tag{A.25}$$

Paschen's law also predicts that breakdown is impossible for values of Pd less than the limiting value $(Pd)_\infty$:

$$\frac{A(Pd)_\infty}{\beta} = 1, \quad V_s \to \infty, \tag{A.26}$$

$$(Pd)_\infty = \frac{\beta}{A} = \frac{(Pd)_{min}}{e}. \tag{A.27}$$

That is, $(Pd)_\infty$ is slightly more than one-third the value of $(Pd)_{min}$. Raizer [25] notes that breakdown does in fact occur for $Pd < (Pd)_\infty$, resulting from field emission of electrons from the cathode.

A.3. Measurements

The starting voltage was measured, and the light output was recorded when observed visually for discharges in He, N_2, and H_2. Measurements were made for varying gas pressures at room and elevated temperatures. The experimental apparatus and setup and the apparatus and methods to provide the driving field and measure the voltage and current of the gas discharge are described in the power cell apparatus and procedure section.

The inside diameter of the stainless-steel cell which formed the outer electrode was $D_0 = 9.21$ cm. The overall diameter of the axial electrode was $D_i = 5.72$ cm. For an electrode potential V, the magnitude of the field strength at a radial distance r from the cell axis, ignoring end effects, was

$$X(r) = \frac{V}{r \log(D_0/D_i)}. \tag{A.28}$$

The ratio of the field strengths at the cell wall and the axial electrode was

$$\frac{X_0}{X_i} = \frac{D_i}{D_0} = 0.621. \tag{A.29}$$

Thus, Paschen's law applied since the field strength did not vary significantly across the discharge gap. The mean field strength was

$$X = \frac{V}{d}, \tag{A.30}$$

where $d = (D_0 - D_i)/2 = 1.75$ cm was the electrode spacing.

The observed and theoretical (Paschen equation (Eqs. (A.20)–(A.21)) starting voltages and the observed maintenance voltages and light emission for helium at 25°C as a function of the helium pressure are shown in Fig. 18. The observed starting and maintenance voltages and light emission for helium at 662°C as a function of the helium pressure are shown in Fig. 19. The starting voltage exhibited the expected minimum with respect to pressure variation. At higher temperature, the starting voltages near the minimum were distributed over a broader range of pressure. By

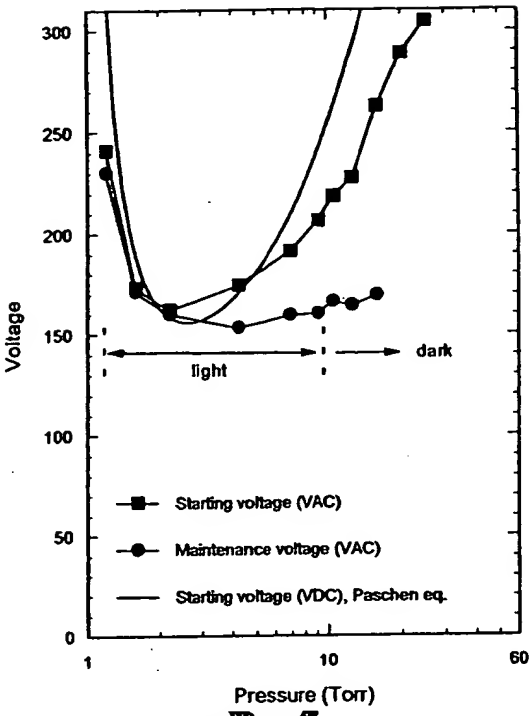

Fig. 18. The observed and theoretical (Paschen equation (Eqs. (A.18)–(A.19)) starting voltages and the observed maintenance voltages and light emission for helium at 25°C as a function of the helium pressure.

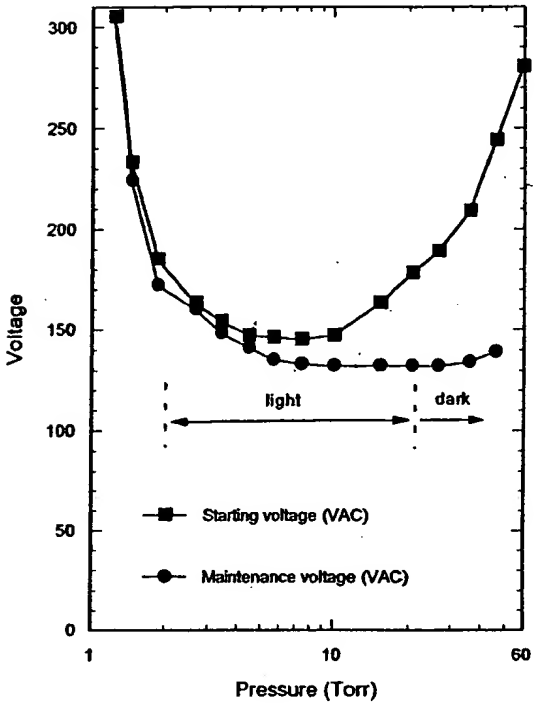

Fig. 19. The observed starting and maintenance voltages and light emission for helium at 662°C as a function of the helium pressure.

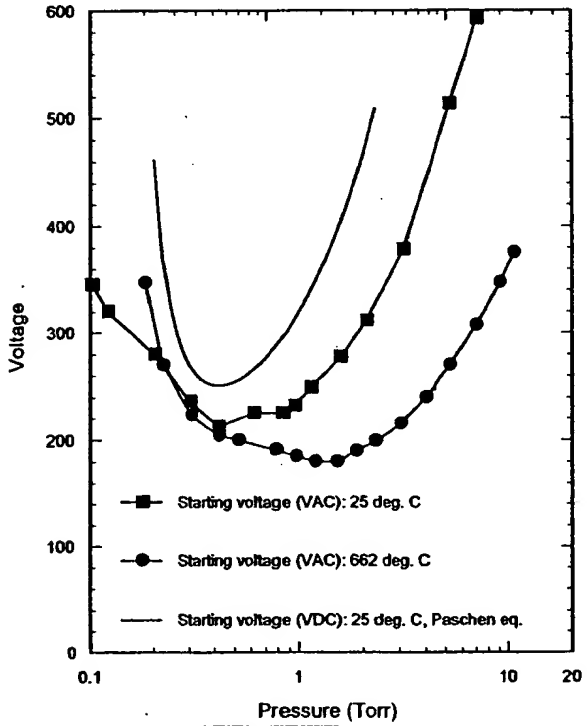

Fig. 20. The observed and theoretical (Paschen equation (Eqs. (A.18)–(A.19)) starting voltages for nitrogen at 25°C as a function of the nitrogen pressure and the observed starting voltages for nitrogen at 662°C as a function of the nitrogen pressure.

increasing temperature to 662°C, the minimum starting voltage, $V_{s\,min}$, was diminished only about 10%. P_{min}, the pressure corresponding to the minimum starting voltage, was shifted toward higher pressure with increasing temperature. However, P_{min} occurred at nearly the same gas number density at 25°C as at 662°C which is in agreement with theory

$$\frac{n_{662°C}}{n_{25°C}} = 1.07. \tag{A.31}$$

At 25°C, $(Pd)_{min} = 3.85$ cm torr which was in good agreement with the published value, $(Pd)_{min}$ = [illegible] cm torr, shown in Table 7. The difference between the starting and maintenance voltage increased for pressures greater than P_{min}. From Fig. 18, the Paschen equation was a good predictor of P_{min}, but it under-predicted the starting voltage by a margin of 10–40%. The discrepancy was masked in Fig. 18 since the peak voltage was a factor of $\sqrt{2}$ greater than the rms value shown. Subsequent to breakdown, a glow discharge was observed for a range of pressures about P_{min}. Light emission from the discharge was greatest for pressures very near P_{min}. For pressures significantly lower than P_{min}, a discharge was formed (conducting gas) with little or no light emission. A similar effect was observed for pressures substantially greater than P_{min}.

The observed and theoretical (Paschen equation (Eqs. (A.20)–(A.21)) starting voltages for nitrogen at 25°C as a function of the nitrogen pressure and the observed starting voltages for nitrogen at 662°C as a function of the nitrogen pressure are shown in Fig. 20. The qualitative features of the breakdown process and the discharge were similar to those of helium. The variation of V_s and P_{min} with temperature and the variation of light emission with pressure were similar. The minimum starting voltage was 35–50 V higher than that of helium, and P_{min} was smaller. At 25°C, $(Pd)_{min} = 0.73$ cm torr while from Table 7 $(Pd)_{min} = 0.67$ cm torr. The Paschen equation was again a good predictor of P_{min}. For nitrogen, the starting voltage was also reasonably well predicted except near P_{min}. The Paschen equation under-predicted the starting voltage by 15–20% when the nitrogen pressure was near P_{min} considering that the actual voltage peaks exceeded the rms voltage by the factor $\sqrt{2}$. The gas number densities at $P = P_{min}$ were in the ratio

$$\frac{n_{662°C}}{n_{25°C}} = 1.03. \tag{A.32}$$

At 662°C, the nitrogen pressure decreased steadily whenever a discharge was present in the cell. Perhaps the increased frequency of nitrogen ion collisions with the electrode surfaces enabled the formation of nitride compounds.

The observed and theoretical (Paschen equation (Eqs. (A.20)–(A.21)) starting voltages for hydrogen at 25°C as a

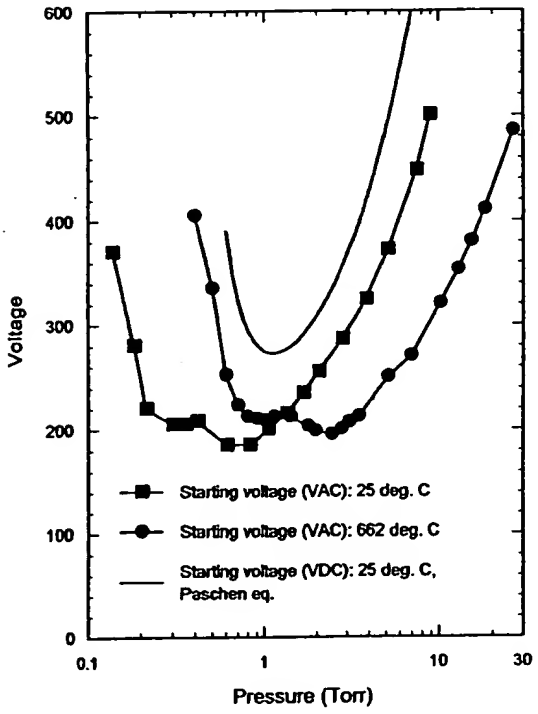

Fig. 21. The observed and theoretical (Paschen equation (Eqs. (A.18)–(A.19)) starting voltages for hydrogen at 25°C as a function of the hydrogen pressure and the observed starting voltages for hydrogen at 662°C as a function of the hydrogen pressure.

function of the hydrogen pressure and the observed starting voltages for hydrogen at 662°C as a function of the hydrogen pressure are shown in Fig. 21. The minimum starting voltages were similar to those observed for nitrogen. However, the variation of V_s with pressure differed from the behavior observed for He and N_2. A local minimum was observed in the $V_s - P$ relation at a pressure slightly below P_{min} of this behavior may result from strong variation of the secondary ionization coefficient γ for hydrogen near $X/P \approx$ [illegible] V/cm-Torr [26]. Also, the broadening effect and the decrease in $V_{s\,min}$ with increased temperature were not observed in the case of hydrogen. In fact, the minimum starting voltage was observed to increase slightly with temperature. As with He and N_2, the V_s curve was shifted toward higher pressure with increasing temperature in order to preserve the number density. The number density ratio at P_{min} was

$$\frac{n_{662°C}}{n_{25°C}} = 1.11. \qquad \text{(A.33)}$$

The Paschen equation over-predicted P_{min}, but it predicted the starting voltage reasonably well for pressures greater than P_{min}. The measured value $(Pd)_{min} = 1.23$ cm torr at 25°C was again in good agreement with 1.15 cm torr given in Table 7. As with nitrogen, the hydrogen pressure decreased steadily when a discharge was present. This effect was observed in hydrogen both at elevated temperature and at room temperature. The pressure may have decreased due to hydride formation.

References

[1] Mills R, Dong J, Lu Y. Observation of extreme ultraviolet hydrogen emission from incandescently heated hydrogen gas with certain catalysts. 1999 Pacific Conference on Chemistry and Spectroscopy and the 35th ACS Western Regional Meeting, Ontario Convention Center, California, October 6–8, 1999.

[2] Mills R, Dong J, Lu Y. Observation of extreme ultraviolet hydrogen emission from incandescently heated hydrogen gas with certain catalysts. Int J Hydrogen Energy 2000;25:919–43.

[3] Mills R. Observation of extreme ultraviolet emission from hydrogen-KI plasmas produced by a hollow cathode discharge. Int J Hydrogen Energy, submitted for publication.

[4] Mills R. Temporal behavior of light-emission in the visible spectral range from a Ti-K2CO3-H-Cell. Int J Hydrogen Energy, in press.

[5] Mills R, Lu Y, Onuma T. Formation of a hydrogen plasma from an incandescently heated hydrogen-potassium gas mixture and plasma decay upon removal of heater power. Int J Hydrogen Energy, in press.

[6] Phillips JH. Guide to the Sun. Cambridge, Great Britain: Cambridge University Press, 1992. p. 16–20.

[7] Sampson JAR. Techniques of vacuum ultraviolet spectroscopy. Pied Publications, 1980. p. 94–179.

[8] Science News 92/6/27, p. 366.

[9] Fujimoto T, Sawada K, Takahata K. J Appl Phys 1989;66(6):2815–9.

[10] Hollander A, Wertheimer MR. J Vac Sci Technol A 1994;12(3):879–82.

[11] Mills R. The grand unified theory of classical quantum mechanics, January 2000 ed. Cranbury, New Jersey: BlackLight Power, Inc., Distributed by Amazon.com.

[12] Sidgwick NV. The chemical elements and their compounds, vol. I. Oxford: Clarendon Press, 1950. p. 17.

[13] Lamb MD. Luminescence spectroscopy. London: Academic Press, 1978. p. 68.

[14] Linde DR. CRC handbook of chemistry and physics, 79th ed., Boca Raton, Fl: CRC Press, 1998–9. p. 10-175–7.

[15] Yaws CL. Chemical properties handbook. New York: McGraw-Hill, 1999.

[16] Linde DR. CRC handbook of chemistry and physics, 79th ed. Boca Raton, Fl: CRC Press, 1998–9. p. 10-1–87.

[17] von Engel A. Ionized gases. American Institute of Physics, 1965.

[18] Naidu MS, Kamaraju V. High voltage engineering. New York: McGraw-Hill, 1996.

[19] Mills R, Dhandapani B, Greenig N, He J. Synthesis and characterization of potassium iodo hydride. Int J Hydrogen Energy, in press.

[20] Mills R. Novel inorganic hydride. Int J Hydrogen Energy 2000;25:669–83.

[21] Mills R. Novel hydrogen compounds from a potassium carbonate electrolytic cell. Fusion Technol 2000;37(2): 157–82.

[22] Mills R, He J, Dhandapani B. Novel hydrogen compounds. 1999 pacific conference on chemistry and spectroscopy and

the 35th ACS Western Regional Meeting, Ontario Convention Center, California, October 6–8, 1999.

[23] Mills R, Dhandapani B, Nansteel M, He J. Synthesis and characterization of novel hydride compounds. Int J Hydrogen Energy, submitted for publication.

[24] Mills R. Highly stable novel inorganic hydrides. J Mater Res., submitted for publication.

[25] Raizer YP. Gas discharge physics. Berlin: Springer, 1997.

[26] Brown SC. Basic data of plasma physics. Cambridge, MA: MIT Press, 1959.